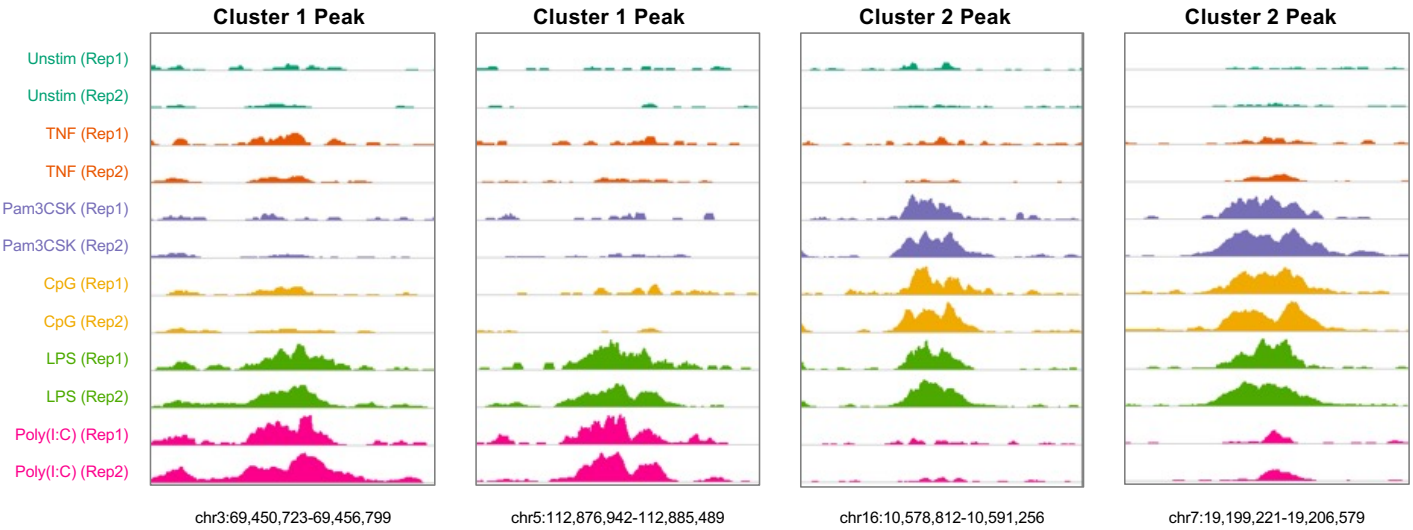


**Fig. S1:** Genome browser tracks of representative H3K4me1 ChIP-seq peaks showing stimulus-specific *de novo* enhancers from Fig. 1A., two replicates per condition.

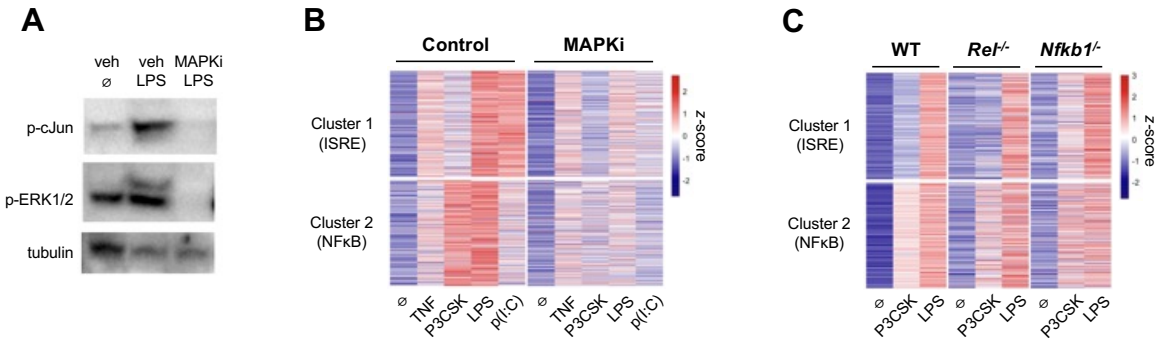


**Fig. S2: Role of MAPK pathway and NFκB subunits on *de novo* enhancers. A)** Western blot for phospho-cJun and phospho-ERK1/2 in BMDMs treated with JNK and MEK1/2 inhibitors (MAPKi) and stimulated with LPS for 30 minutes. **B)** Heat map of H3K4me1 ChIP-seq signal across Cluster 1 and 2 regions as defined in Fig. 1A after eight hours stimulation, showing effect of MAPK inhibitors. **C)** Heat map of H3K4me1 ChIP-seq signal in wild-type (WT), cRel knockout (*Rel*$^{-/-}$), and p50 knockout (*Nfkb1*$^{-/-}$) BMDMs stimulated for eight hours with indicated ligands.

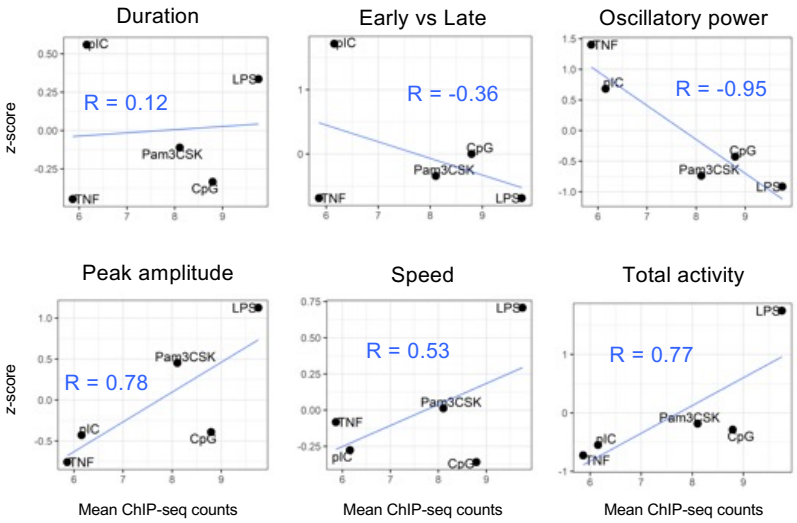


**Fig. S3: Correlation of NFκB dynamics to ChIP-seq data.** Scatterplots and Pearson's correlation of mean ChIP-seq counts in NFκB enhancer regions (Fig 1D) *vs.* stimulus-specific z-scores for each of the six key features of NFκB signaling dynamics.

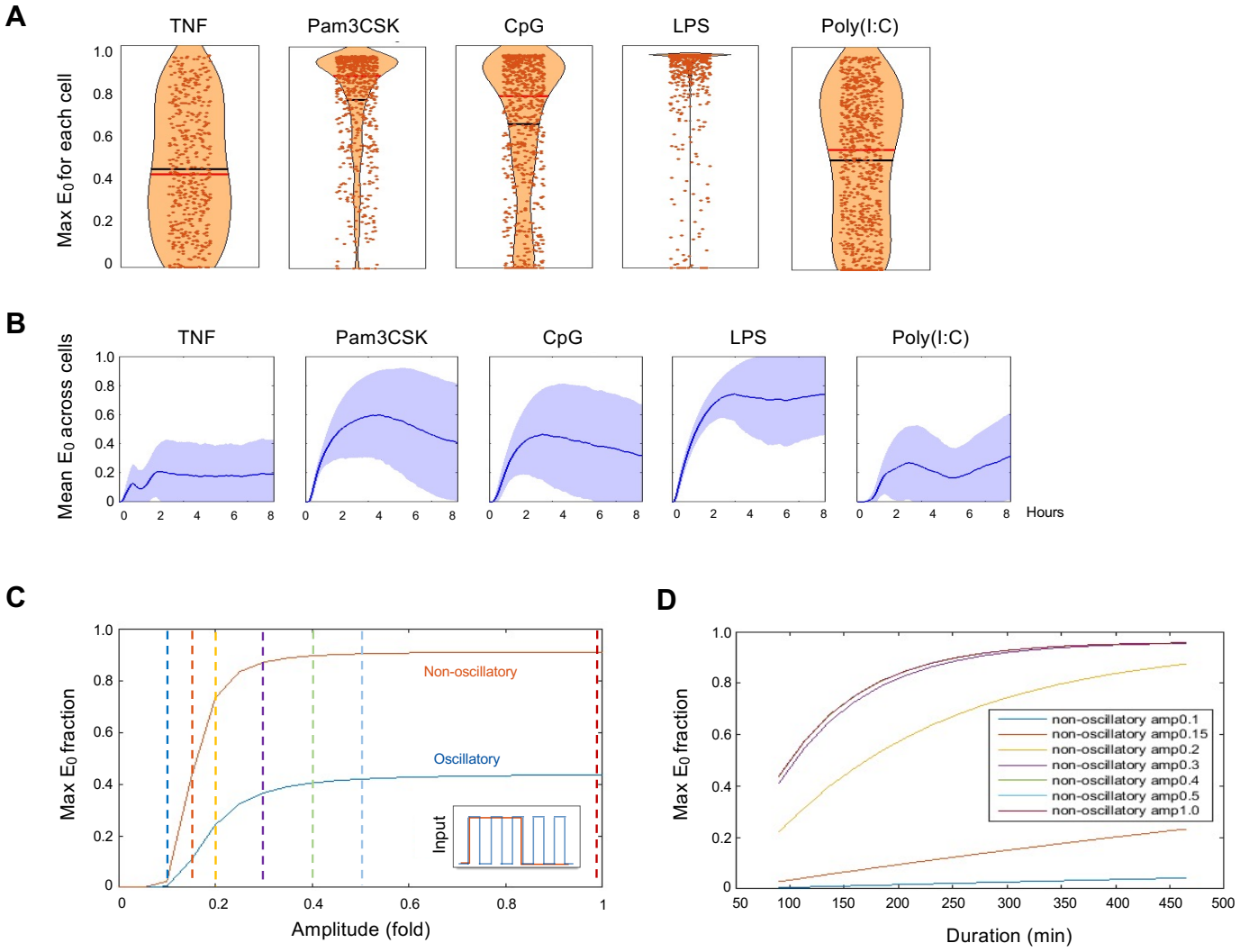


**Fig. S4: Supplemental model simulations. A)** Violin plots of maximum chromatin opening over eight hours per single-cell stimulation, using NFκB trajectories as input to the model. Black line = mean, Red line = median. **B)** Simulated mean chromatin opening over time across all single cells. **C)** Model simulations across a range of NFκB amplitudes, comparing oscillatory and non-oscillatory trajectories. **D)** Model simulations across a range of NFκB durations, comparing a range of NFκB amplitudes marked by dotted lines in Panel (C).

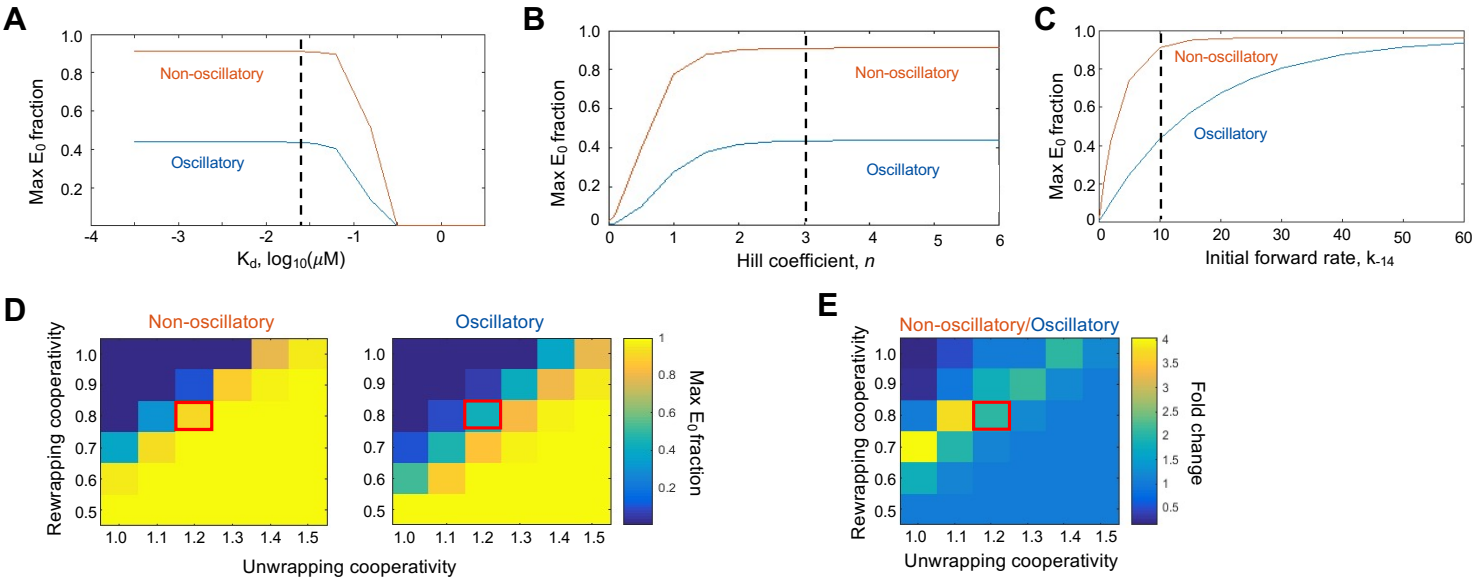


**Fig. S5: Parameter sensitivity analysis. A)** Chromatin opening behavior when the model is tested across a range of $K_D$s, **B)** across a range of Hill coefficients, or **C)** across a range of forward rates for the first unwrapping step, $k_{-14}$. For model simulations (Fig. 2D), $K_D$ = 0.025, Hill = 3, and $k_{-14}$ = 10 were used, marked by the dotted black line. **D-E)** Heat map of chromatin opening across a range of unwrapping and rewrapping cooperativity factors, showing maximum $E_0$ fraction in non-oscillatory and oscillatory conditions (D) and fold change difference between maximum non-oscillatory and oscillatory conditions (E). Red box indicates the parameter values used for model simulations.

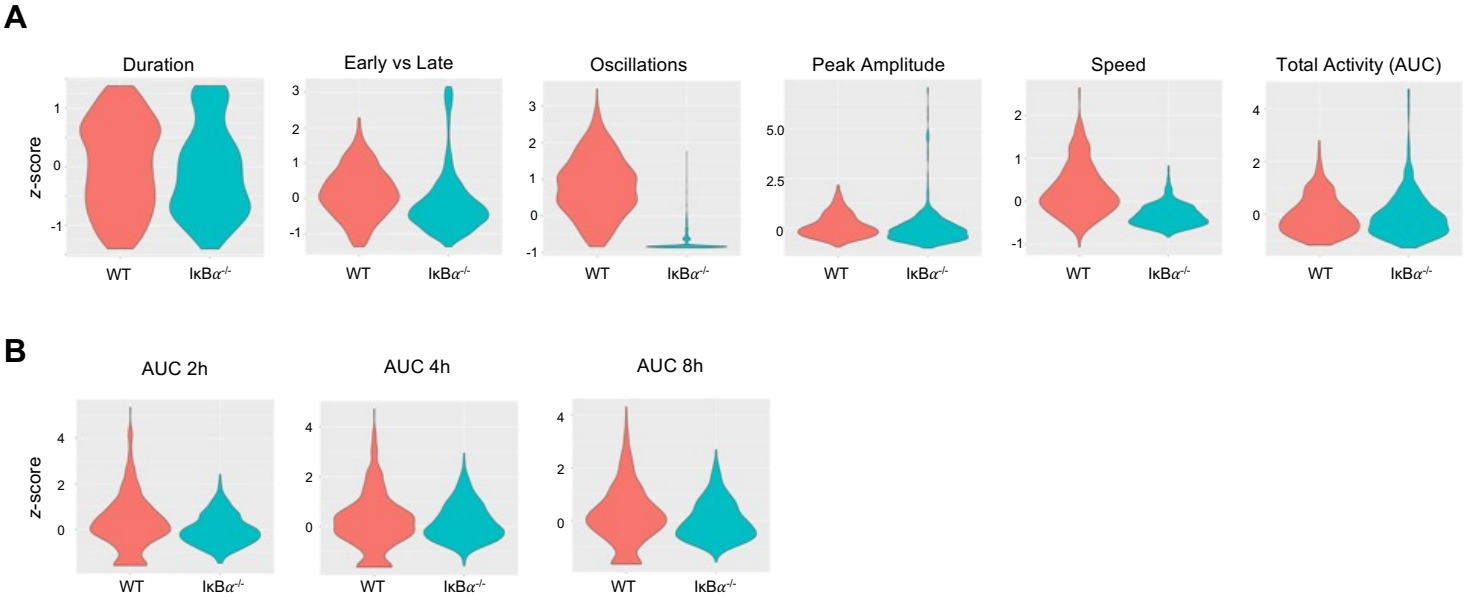


**Fig. S6: NFκB dynamics in TNF-stimulated IκBα$^{-/-}$ vs WT BMDMs. A)** Violin plots of single-cell distributions for the six key NFκB signaling features. **B)** Violin plots of single-cell distributions for areas under the NFκB activity curve at two, four, and eight hours.

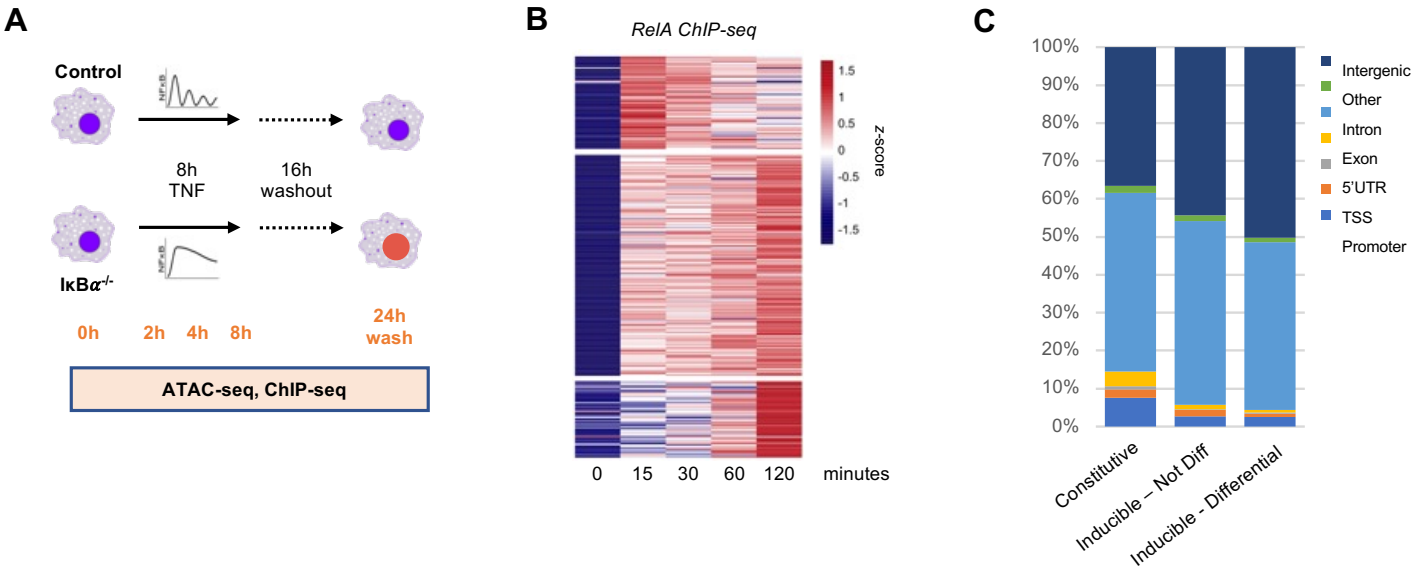


**Fig. S7: Supplemental ATAC-seq data. A)** Schematic of ATAC and ChIP-seq experiments in IκB$\alpha^{-/-}$ and control BMDMs. **B)** Heat map of Lipid A-stimulated NFκB RelA ChIP-seq signal *(25)* at 322 inducible-differential ATAC-seq regions, 311 of which overlap with a RelA ChIP-seq peak. **C)** Genomic distribution of three categories of accessible regions identified by ATAC-seq.

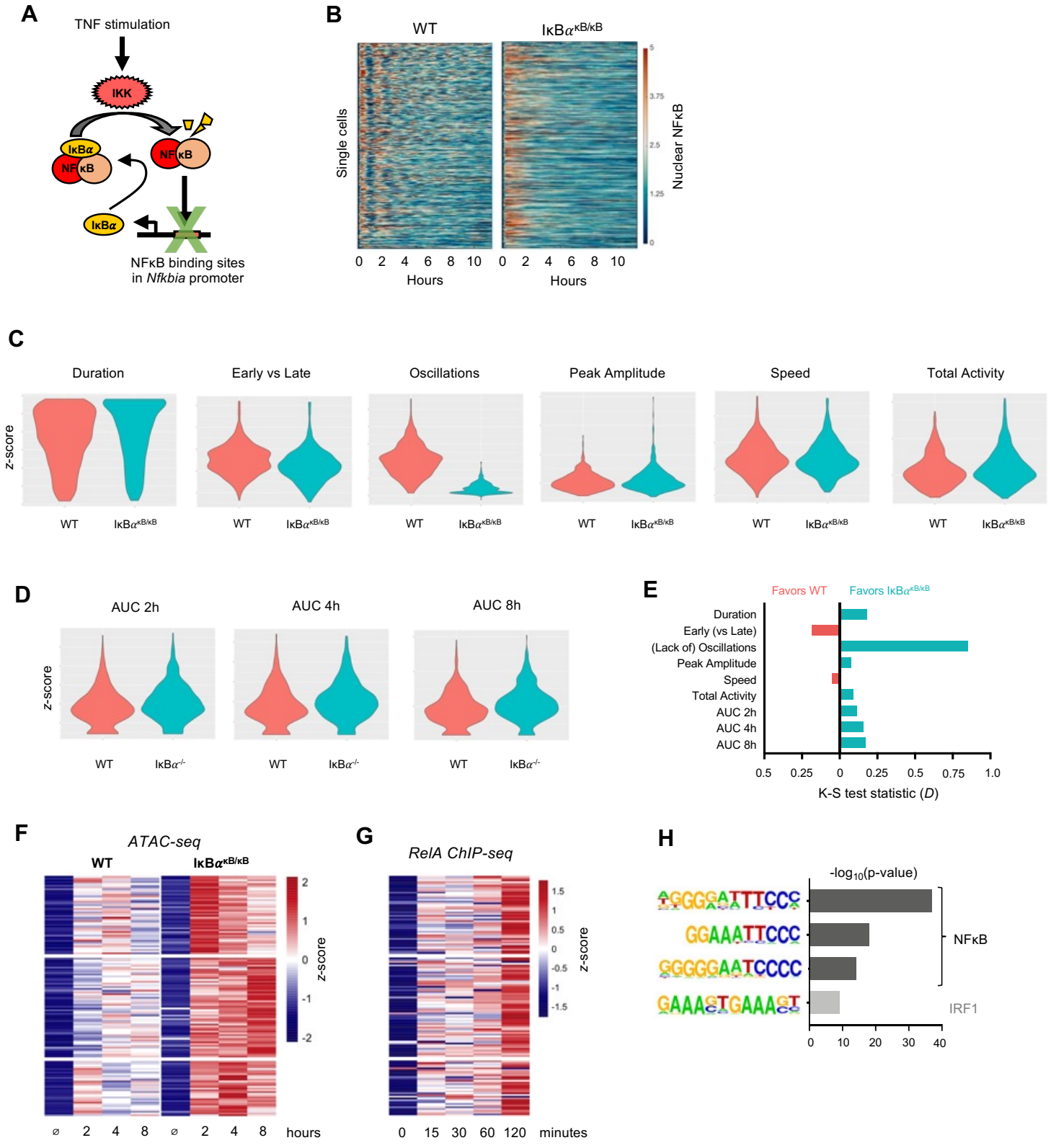


**Fig. S8: *Nfkbia*$^{\kappa B/\kappa B}$ mutant as a complementary model of non-oscillatory NFκB. A)** Schematic of *Nfkbia*$^{\kappa B/\kappa B}$ mutation, abolishing inducible IκB$\alpha$ by disrupting NFκB binding sites in promoter *(26)*. **B)** Heat map of single cell NFκB trajectories by microscopy, comparing TNF response in WT *vs.* IκB$\alpha^{\kappa B/\kappa B}$ BMDMs. **C)** Violin plots of single-cell distributions for the six key NFκB signaling features. **D)** Violin plots of single-cell distributions for areas under the NFκB activity curve at two, four, and eight hours. **E)** Bar graph of K-S test statistic for difference in distribution of six key signaling features and areas under NFκB activity curve (AUC), comparing IκB$\alpha^{\kappa B/\kappa B}$ and WT. **F)** Heat map of ATAC-seq signal at 131 genomic regions that are TNF-inducible and differential between IκB$\alpha^{\kappa B/\kappa B}$ and WT. Average of two replicates. **G)** Heat map of Lipid-A stimulated NFκB RelA ChIP-seq signal *(25)* at 131 inducible-differential ATAC-seq regions, 118 of which overlap with a RelA ChIP-seq peak. **H)** Known transcription factor motifs with greatest enrichment in differentially inducible ATAC-seq regions.

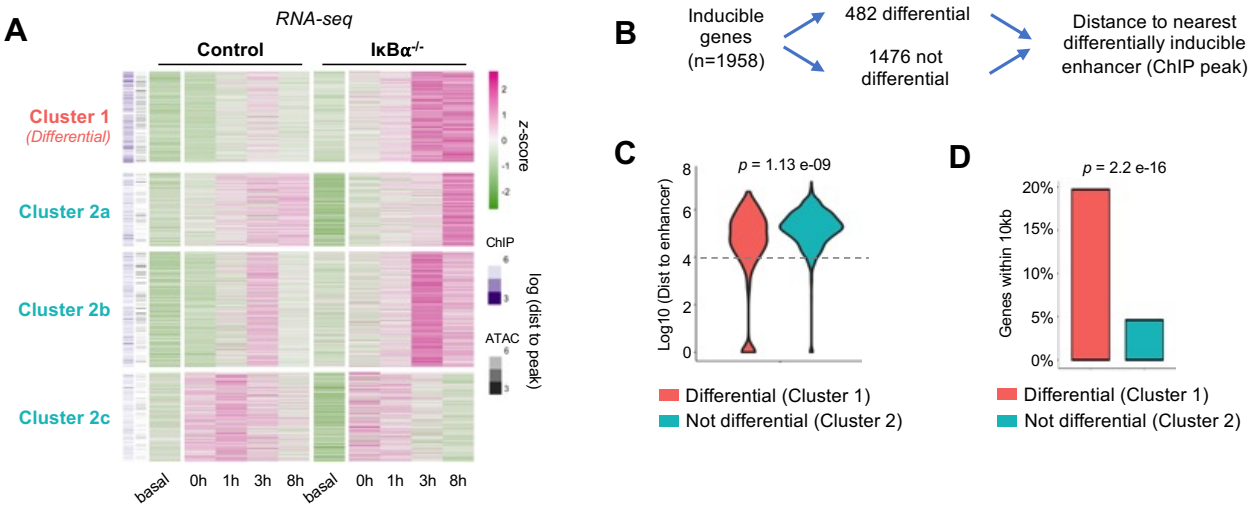


**Fig. S9: Gene-centric approach to investigate the function of dynamics-dependent enhancers. A)** Heat map of TNF-inducible genes in control or IκB$\alpha^{-/-}$ BMDMs (n=1958), average of two replicates. Cluster 1 genes are differentially induced between IκB$\alpha^{-/-}$ and control. Clusters 2a-2c genes are inducible but not differential. **B)** Gene-centric approach to map inducible genes to nearest dynamics-dependent enhancers. **C)** Violin plots of distance from gene TSS to nearest differentially inducible enhancer, comparing genes in Cluster 1 (differential) and Cluster 2 (not differential) by K-S test. **D)** Percentage of genes in each cluster within 10kb (dashed line, panel C) of a differentially inducible enhancer, evaluated by *chi* square test.